

On the augmented Biot-JKD equations with Pole-Residue representation of the dynamic tortuosity

Miao-Jung Yvonne Ou^{†,1}, Hugo J. Woerdeman^{‡2},

[†]Department of Mathematical Sciences, University of Delaware, Newark, DE 19716, USA,
mou@udel.edu

[‡]Department of Mathematics, Drexel University, Philadelphia, PA 19104, USA,
hugo@math.drexel.edu

Dedicated to our colleague and friend Joe Ball

Abstract

In this paper, we derive the augmented Biot-JKD equations, where the memory terms in the original Biot-JKD equations are dealt with by introducing auxiliary dependent variables. The evolution in time of these new variables are governed by ordinary differential equations whose coefficients can be rigorously computed from the JKD dynamic tortuosity function $T^D(\omega)$ by utilizing its Stieltjes function representation derived in [14], where an algorithm for computing the pole-residue representation of the JKD tortuosity is also proposed. The two numerical schemes presented in the current work for computing the poles and residues representation of $T^D(\omega)$ improve the previous scheme in the sense that they interpolate the function at infinite frequency and have much higher accuracy than the one proposed in [14].

1 Introduction

Biot equations are governing equations for wave propagation in linear poroelastic media. The first-order formulation of the Biot's equations consists of the strain-stress relations of the poroelastic materials and the equations of motion in terms of the solid displacement \mathbf{u} , the pore fluid velocity relative to the solid \mathbf{q} and the pore pressure p . The first-order formulation of Biot-JKD equations consists of the stress rate-strain rate relations and the dynamic equations. In terms of the solid displacement \mathbf{u} , we define the following variables

$$\mathbf{v} := \partial_t \mathbf{u} \text{ (solid velocity) , } \mathbf{w} := \phi(\mathbf{U} - \mathbf{u}) \text{ (fluid displacement relative to the solid) , } \mathbf{q} := \partial_t \mathbf{w}, \zeta := -\nabla \cdot \mathbf{w}$$

where ϕ is the porosity. Here \mathbf{U} is the averaged fluid velocity over a representative volume element. The spatial coordinates (x_1, x_2, x_3) are chosen to be aligned with the principal directions of the static permeability tensor \mathbf{K} of the poroelastic material, which is known to be symmetric and positive definite.

Let $\epsilon_{ij} := \frac{1}{2}(\frac{\partial u_i}{\partial x_j} + \frac{\partial u_j}{\partial x_i})$ be the linear strain of the solid part, then the stress-strain relation is given by [4]

$$\begin{pmatrix} \sigma_{11} \\ \sigma_{22} \\ \sigma_{33} \\ \sigma_{23} \\ \sigma_{13} \\ \sigma_{12} \\ p \end{pmatrix} = \begin{pmatrix} c_{11}^u & c_{12}^u & c_{13}^u & c_{14}^u & c_{15}^u & c_{16}^u & M\alpha_1 \\ c_{12}^u & c_{22}^u & c_{23}^u & c_{24}^u & c_{25}^u & c_{26}^u & M\alpha_2 \\ c_{13}^u & c_{23}^u & c_{33}^u & c_{34}^u & c_{35}^u & c_{36}^u & M\alpha_3 \\ c_{14}^u & c_{24}^u & c_{34}^u & c_{44}^u & c_{45}^u & c_{46}^u & M\alpha_4 \\ c_{15}^u & c_{25}^u & c_{35}^u & c_{45}^u & c_{55}^u & c_{56}^u & M\alpha_5 \\ c_{16}^u & c_{26}^u & c_{36}^u & c_{46}^u & c_{56}^u & c_{66}^u & M\alpha_6 \\ M\alpha_1 & M\alpha_2 & M\alpha_3 & M\alpha_4 & M\alpha_5 & M\alpha_6 & M \end{pmatrix} \begin{pmatrix} \epsilon_{11} \\ \epsilon_{22} \\ \epsilon_{33} \\ 2\epsilon_{23} \\ 2\epsilon_{13} \\ 2\epsilon_{12} \\ -\zeta \end{pmatrix} \quad (1)$$

where p is the pore pressure, c_{ij}^u are the elastic constants of the undrained frame, which are related to the elastic constants c_{ij} of the drained frame by $c_{ij}^u = c_{ij} + Ma_i a_j$, $i, j = 1, \dots, 6$. In terms of the material bulk

¹The work of MYO is partially sponsored by NSF-DMS-1413039

²HJW is partially supported by Simons Foundation grant 355645

moduli κ_s and κ_f of the solid and the fluid, respectively, the fluid-solid coupling constants a_i and M are given by

$$a_i := \begin{cases} 1 - \frac{1}{3\kappa_s} \sum_{k=1}^3 c_{ik} & \text{for } i = 1, 2, 3, \\ -\frac{1}{3\kappa_s} \sum_{k=1}^3 c_{ki} & \text{for } i = 4, 5, 6, \end{cases}$$

$$M := \frac{\kappa_s}{1 - \bar{\kappa}/\kappa_s - \phi(1 - \kappa_s/\kappa_f)},$$

$$\bar{\kappa} := \frac{c_{11} + c_{22} + c_{33} + 2c_{12} + 2c_{13} + 2c_{23}}{9}.$$

The six equations of motion are as follows

$$\sum_{k=1}^3 \frac{\partial \sigma_{jk}}{\partial x_k} = \rho \frac{\partial v_j}{\partial t} + \rho_f \frac{\partial q_j}{\partial t}, \quad t > 0, \quad (2)$$

$$-\frac{\partial p}{\partial x_j} = \rho_f \frac{\partial v_j}{\partial t} + \left(\frac{\rho_f}{\phi} \right) \check{\alpha}_j \star \frac{\partial q_j}{\partial t}, \quad t > 0, \quad j = 1, 2, 3, \quad (3)$$

where \star denotes the time-convolution operator, ρ_f and ρ_s are the density of the pore fluid and of the solid, respectively, $\rho := \rho_s(1 - \phi) + \phi\rho_f$ and $\check{\alpha}_j$ is the inverse Laplace transform of the dynamic tortuosity $\alpha_j(\omega)$ with ω being the frequency. Here the one-sided Laplace transform of a function $f(t)$ is defined as

$$\hat{f}(\omega) := \mathcal{L}[f](s = -i\omega) := \frac{1}{\sqrt{2\pi}} \int_0^\infty f(t) e^{-st} dt.$$

As a special case of the Biot-JKD equations, the low frequency Biot's equation corresponds to

$$\check{\alpha}_j(t) = \alpha_{\infty j} \delta(t) + \frac{\eta\phi}{K_{0j}\rho_f} H(t),$$

where $\delta(t)$ is the Dirac function and $H(t)$ the Heaviside function, η the dynamic viscosity of the pore fluid, K_{0j} the static permeability in the x_j direction. This low-frequency tortuosity function corresponds to

$$\alpha_j(\omega) = \alpha_{\infty j} + \frac{\eta\phi/K_{0j}\rho_f}{-i\omega}.$$

According to Theorem 5.1 in [14], in the principal coordinates $\{x_j\}_{j=1}^3$ and for ω such that $-\frac{i}{\omega} \in \mathbb{C} \setminus \theta_1$, the dynamic tortuosity function has the following integral representation formula

$$T_j(\omega) = a_j \left(\frac{i}{\omega} \right) + \int_0^{\theta_1} \frac{d\sigma_j(t)}{1 - i\omega t}, \quad a_j := \frac{\eta\phi}{\rho_f K_{0j}}, \quad j = 1, 2, 3, \quad (4)$$

where $0 < \theta_1 < \infty$ and the positive measure $d\sigma_j$ has a Dirac measure of strength $\alpha_{\infty j}$ sitting at $t = 0$; this is to take into account the asymptotic behavior of dynamic tortuosity as frequency goes to ∞ . This function is the analytic continuation of the usual dynamic tortuosity function in which $\omega \geq 0$. As a function of the new variable $s := -i\omega$, $\omega \in \mathbb{C}$, the singularities of (4) are included in the interval $(-\infty, -\frac{1}{\theta_1})$ and a simple pole sitting at $s = 0$. Therefore, if we define a new function for each $j = 1, 2, 3$

$$D_j(s) := T_j(\omega) - \frac{ia_j}{\omega} = \int_0^{\theta_1} \frac{d\sigma_j(t)}{1 + st}, \quad (5)$$

then $D_j(s)$ is analytic in $\mathbb{C} \setminus (-\infty, -\frac{1}{\theta_1})$ on the s -plane. This type of functions are closely related to the well-known Stieltjes functions. The first algorithm we propose in this paper is based on the fact [10] that a Stieltjes function can be well approximated by its Padé approximant whose poles are all simple. The other algorithm proposed here for computing the pole-residue approximation of the dynamic tortuosity function is based on the result in [1].

The main result of this paper is on how to utilize this analytical property of the dynamic tortuosity function to develop an efficient time-domain solver for the Biot-JKD equations, in which the dynamic tortuosity function is proposed by Johnson, Koplik and Dashen in [12] and is defined as follows

$$T^J(\omega) = \alpha_\infty \left(1 - \frac{\eta\phi}{i\omega\alpha_\infty\rho_f K_0} \sqrt{1 - i \frac{4\alpha_\infty^2 K_0^2 \rho_f \omega}{\eta\Lambda^2 \phi^2}} \right), \quad (6)$$

with the tunable geometry-dependent constant Λ . We note that the tortuosity-permeability relation $T(\omega) = \frac{i\eta\phi}{\omega\rho_f} K^{-1}(\omega)$ implies the corresponding permeability is

$$K^J(\omega) = K_0 / \left(\sqrt{1 - \frac{4i\alpha_\infty^2 K_0^2 \rho_f \omega}{\eta\Lambda^2 \phi^2}} - \frac{i\alpha_\infty K_0 \rho_f \omega}{\eta\phi} \right), \quad (7)$$

where $\eta = \rho_f \nu$ is the dynamic viscosity of pore fluid. We refer to $T^J(\omega)$ as the JKD tortuosity function. To separate the simple pole of T^J from the other singularities, we define a new function D^J such that

$$D^J(s) := \alpha_\infty \left(1 + \frac{\eta\phi}{s\alpha_\infty\rho_f K_0} \sqrt{1 + s \frac{4\alpha_\infty^2 K_0^2 \rho_f}{\eta\Lambda^2 \phi^2}} \right) - \frac{a}{s} =: \alpha^J(s) - \frac{a}{s}.$$

It is shown in [14] that $D(s)$ is a Stieltjes function analytic away from the branch cut $[0, C_1]$ along the real axis, where $C_1 := \frac{4\alpha_\infty^2 K_0^2}{\nu\phi^2\Lambda^2}$, and the JKD dynamic tortuosity function indeed can be written as an integral representation

$$T_j^J(\omega) = a \left(\frac{i}{\omega} \right) + \int_0^{\theta_1} \frac{d\sigma_j^J(t)}{1 - i\omega t}, \quad \omega \in \mathbb{R}, \quad (8)$$

where $\theta_1 = C_1$. In other words,

$$D_j^J(s) = \int_0^{\theta_1} \frac{d\sigma_j^J(t)}{1 + st} \approx \alpha_\infty + \sum_{k=1}^M \frac{r_k^j}{s - p_k^j} \text{ for } s \in \mathbb{C} \setminus (-\infty, -\frac{1}{C_1}], j = 1, 2, 3. \quad (9)$$

with $r_k^j > 0$, $p_k^j < -\frac{1}{C_1} < 0$, $j = 1, 2, 3$, $k = 1, \dots, M$, that can be computed from dynamic permeability data $K(\omega)$ evaluated at M different frequencies in the frequency content of the initial waves. The special choice of $s = -i\omega$, $\omega \in \mathbb{R}$ in (9) provides a pole-residue approximation of $T^J(\omega)$.

Applying Laplace transform to the convolution term in (3) with JKD tortuosity, i.e. $\alpha = \alpha^J$, (see eg. Theorem 9.2.7 in [7])

$$\mathcal{L}[\alpha^J \star \frac{\partial q_j}{\partial t}](s) = \alpha^J(s)(s\hat{q}_j) \quad (10)$$

$$= \left(D^J(s) + \frac{a}{s} \right) (s\hat{q}_j) \quad (11)$$

$$\approx \left(\alpha_\infty + \sum_{k=1}^M \frac{r_k}{s - p_k} + \frac{a}{s} \right) (s\hat{q}_j) \quad (12)$$

$$\approx \alpha_\infty s\hat{q}_j + \sum_{k=1}^M \frac{r_k}{s - p_k} (s\hat{q}_j) + a\hat{q}_j \quad (13)$$

$$= \alpha_\infty s\hat{q}_j + \left(a + \sum_{k=1}^M r_k \right) \hat{q}_j + \sum_{k=1}^M r_k p_k \frac{\hat{q}_j}{s - p_k}. \quad (14)$$

Notice that

$$s\hat{q}_j = \mathcal{L} \left[\partial_t q^j \right] + q_j(0). \quad (15)$$

Furthermore, for each of the terms in the sum, since all the singularities p_k are restricted to the left of $s = -\frac{1}{C_1}$, the inverse Laplace transform can be performed by integrating along the imaginary axis for $t > 0$, i.e.,

$$\mathcal{L}^{-1} \left[\frac{1}{s - p_k} \right] (t) = \frac{1}{\sqrt{2\pi}} \int_{-i\infty}^{i\infty} \frac{1}{\zeta - p_k} e^{\zeta t} d\zeta = r_k e^{p_k t}, \quad t > 0.$$

This integral is evaluated by integrating along $[-Ri, Ri] \cup \{s = Re^{i\theta}|\pi/2 < \theta < 3\pi/2\}$ and applying the residue theorem and letting $R \rightarrow \infty$ (see Appendix 1). As a result, we have for $t > 0$

$$\left(\check{\alpha}^J \star \frac{\partial q_j}{\partial t} \right) (\mathbf{x}, t) := \int_0^t \check{\alpha}^J(\tau) \frac{\partial q_j}{\partial t} (\mathbf{x}, t - \tau) d\tau \quad (16)$$

$$\approx \alpha_\infty \left(\frac{\partial q_j}{\partial t} + \delta(0)q_j(0) \right) + \left(a + \sum_{k=1}^M r_k \right) q_j - \sum_{k=1}^M r_k (-p_k) e^{p_k t} \star q_j. \quad (17)$$

Applying a strategy similar to those in the literature [6], we define the auxiliary variables Θ_k , $k = 1, \dots, M$ such that

$$\Theta_k^{x_j} (\mathbf{x}, t) := (-p_k) e^{p_k t} \star q_j. \quad (18)$$

It can be easily checked that Θ_k , $k = 1, \dots, M$, satisfies the following equation:

$$\partial_t \Theta_k^{x_j} (\mathbf{x}, t) = p_k \Theta_k^{x_j} (\mathbf{x}, t) - p_k q_j (\mathbf{x}, t). \quad (19)$$

For an anisotropic media, each principal direction x_j , $j = 1, 2, 3$, has a different tortuosity function α_j . We label the corresponding poles and residue as $p_k^{x_j}$ and $r_k^{x_j}$ and modify (18) accordingly. Replacing the convolution terms in (3) with the equations of $\Theta_k^{x_j}$, we obtain the following system that has no explicit memory terms:

$$\left\{ \begin{array}{l} \sum_{k=1}^3 \frac{\partial \sigma_{jk}}{\partial x_k} = \rho \frac{\partial v_j}{\partial t} + \rho_f \frac{\partial q_j}{\partial t}, \quad t > 0, \quad (20) \\ \partial_t \Theta_k^{x_j} (\mathbf{x}, t) = p_k \Theta_k^{x_j} (\mathbf{x}, t) - p_k q_j (\mathbf{x}, t), \quad j = 1, 2, 3, \quad (21) \\ -\frac{\partial p}{\partial x_j} = \rho_f \frac{\partial v_j}{\partial t} + \left(\frac{\rho_f \alpha_{\infty j}}{\phi} \right) \frac{\partial q_j}{\partial t} + \left(\frac{\eta}{K_{0j}} + \frac{\rho_f}{\phi} \sum_{k=1}^M r_k \right) q_j \\ - \left(\frac{\rho_f}{\phi} \right) \sum_{k=1}^M r_k \Theta_k^{x_j} + \delta(t) \frac{\rho_f \alpha_{\infty j}}{\phi} q_j (\mathbf{x}, 0), \quad t > 0, \quad j = 1, 2, 3. \quad (22) \end{array} \right.$$

We refer to this system as the augmented system of Biot-JKD equations in the principal directions. By the definition of dynamic tortuosity and dynamic permeability it is clear that the principal directions coincide.

2 Numerical scheme for computing r_k and p_k

Since the function D^J results from subtracting the pole of T^J at $s = 0$, it has a removable singularity at $s = 0$ and is analytic away from its branch-cut located at $(-\infty, -1/C_1]$. Both algorithms presented here are based on the fact that $D^J(s)$ is a Stieltjes function.

The problem to be solved is formulated as follows. Given the data of D^J at distinct values of $s = s_1, \dots, s_M$, construct the pole-residue approximation of D^J such that

$$D^J(s) \approx D_{est}^J(s) := \alpha_\infty + \sum_{k=1}^M \frac{r_k}{s - p_k} \quad \text{for } s \in [s_1, s_M] \text{ and } r_k > 0, p_k < 0, \forall k = 1, \dots, M. \quad (23)$$

2.1 Rational function approximation and partial fraction decomposition

This approximation takes into account the asymptotic behavior $\lim_{s \rightarrow \infty} = \alpha_\infty$ and hence can be considered as an improved version of the reconstruction algorithm for tortuosity in [14], which does not interpolate at infinity. In this paper, we also take into account the asymptotic behaviors of $D(s)$. Note that

$$\lim_{\omega \rightarrow 0^+} D(s = -i\omega) = \alpha_\infty + 2 \left(\frac{\alpha_\infty}{\Lambda} \right)^2 \frac{K_0}{\phi}, \quad \lim_{\omega \rightarrow \infty} D(s = -i\omega) = \alpha_\infty \quad (24)$$

By a theorem in [10], we know that the poles in the Padé approximant of $D^J(s)$ have to be contained in $(-\infty, -1/C_1]$ and are all simple with positive weight (residue), this implies that the constant term in the denominator in the Padé approximant can be normalized to one. According to the aforementioned theorem, if $(s, D^J(s))$ is an interpolation point with $Im(s) \neq 0$, then $(\bar{s}, D^J(\bar{s}))$ must also be an interpolation point, where $\bar{\cdot}$ represents the complex conjugate. From the integral representation formula (IRF), we know that $D^J(\bar{s}_k) = \overline{D^J(s_k)}$.

Hence, the following approximation problem is considered: Given M data points $D^J(s_k = -i\omega_k) \in \mathbb{C}$, $k = 1, \dots, M$, find $\mathbf{x} := (a_0, \dots, a_{M-1}, b_1, \dots, b_M)^t$ such that

$$(S) \begin{cases} D^J(s_k) - \alpha_\infty = \frac{a_0 + a_1 s_k + \dots + a_{M-1} s_k^{M-1}}{1 + b_1 s_k + \dots + b_M s_k^M}, k = 1, \dots, M, \\ \overline{D^J(s_k)} - \alpha_\infty = \frac{a_0 + a_1 \bar{s}_k + \dots + a_{M-1} \bar{s}_k^{M-1}}{1 + b_1 \bar{s}_k + \dots + b_M \bar{s}_k^M}, k = 1, \dots, M, \end{cases}$$

where $\omega_k, k = 1, \dots, M$, are distinct positive numbers. However, with a closer look, this system of equations is equivalent to the one by enforcing the condition $\mathbf{x} \in \mathbb{R}^{2M}$ to the first half of (S). To be more specific, we define

$$\begin{aligned} A &:= \begin{pmatrix} 1 & s_1 & s_1^2 & \dots & s_1^{M-1} & -D^J(s_1)s_1 & -D^J(s_1)s_1^2 & \dots & -D^J(s_1)s_1^M \\ 1 & s_2 & s_2^2 & \dots & s_2^{M-1} & -D^J(s_2)s_2 & -D^J(s_2)s_2^2 & \dots & -D^J(s_2)s_2^M \\ \vdots & \vdots & \vdots & & \vdots & \vdots & \vdots & & \vdots \\ 1 & s_M & s_M^2 & \dots & s_M^{M-1} & -D^J(s_M)s_M & -D^J(s_M)s_M^2 & \dots & -D^J(s_M)s_M^M \end{pmatrix} \in \mathbb{C}^{M \times 2M}, \\ \mathbf{d} &:= (D^J(s_1) \ D^J(s_2) \ \dots \ D^J(s_M))^t \in \mathbb{C}^M, \\ \mathbf{x} &:= (a_0, \dots, a_{M-1}, b_1, \dots, b_M)^t \in \mathbb{R}^M. \end{aligned} \quad (25)$$

Then the system to be solved is

$$\begin{pmatrix} Re(A) \\ Im(A) \end{pmatrix} \mathbf{x} = \begin{pmatrix} Re(\mathbf{d}) \\ Im(\mathbf{d}) \end{pmatrix}, \quad (26)$$

where $Re()$ and $Im()$ denote the real part and the imaginary part, respectively. After solving for \mathbf{x} , the poles and residues are then obtained by the partial fraction decomposition of the Padé approximant, i.e.

$$\frac{a_0 + a_1 s + \dots + a_M s^{M-1}}{1 + b_1 s + \dots + b_M s^M} = \sum_{j=1}^M \frac{r_j}{s - p_j}. \quad (27)$$

2.2 Two-sided residue interpolation in the Stieltjes class

The second algorithm is based on the following theorem that can be considered as a special case of what is proved in [1]. The advantage of this method is that it explicitly identifies the poles $p_k, k = 1, \dots, M$ as the generalized eigenvalues of matrices constructed from the data. We note that the interpolation problem below also appears in the recent paper [2], where the main focus is model reduction.

Let $\mathbb{C}^+ := \{z \in \mathbb{C} : Im(z) > 0\}$. Given M interpolation data $(z_i, u_i, v_i) \in \mathbb{C}^+ \times \mathbb{C}^{p \times q} \times \mathbb{C}^{p \times q}$, we seek a $p \times p$ matrix valued function $F(z)$ of the form

$$F(z) = \int_0^\infty \frac{d\mu(t)}{t - z}, \quad \text{where } \mu \text{ is a positive } p \times p \text{ matrix-valued measure} \quad (28)$$

such that

$$F(z_i)u_i = v_i, i = 1, \dots, M. \quad (29)$$

Theorem 2.1. *If there exists a solution $F(z)$ described as above, then the Hermitian matrices S_1 and S_2 defined via*

$$(S_1)_{ij} = \frac{u_i^* v_j - v_i^* u_j}{z_j - \bar{z}_i}, \quad (S_2)_{ij} := \frac{z_j u_i^* v_j - \bar{z}_i v_i^* u_j}{z_j - \bar{z}_i}, \quad i, j = 1, \dots, M, \quad (30)$$

are positive semidefinite. Conversely, if S_1 is positive definite and S_2 is positive semidefinite, then

$$F(z) := -C_+(zS_1 - S_1A - C_+^*C_-)^{-1}C_+^* = C_+(S_2 - zS_1)^{-1}C_+^* \quad (31)$$

is a solution to the interpolation problem. Here

$$C_- := (u_1 \ \cdots \ u_M), \quad C_+ := (v_1 \ \cdots \ v_M), \quad A := \text{diag}(z_i I_q)_{i=1}^M,$$

and I_q is the identity matrix of dimension q .

Proof. Suppose (28) and (29) are true. Then we have

$$u_i^* v_j - v_i^* u_j = u_i^* (F(z_j) - F(z_i)^*) u_j = (z_j - \bar{z}_i) u_i^* \left(\int_0^\infty \frac{d\mu(t)}{(t - z_j)(t - \bar{z}_i)} \right) u_j.$$

Thus

$$S_1 = \int_0^\infty \begin{pmatrix} \frac{u_1^*}{t - \bar{z}_1} \\ \vdots \\ \frac{u_M^*}{t - \bar{z}_M} \end{pmatrix} d\mu(t) \begin{pmatrix} \frac{u_1}{t - z_1} & \cdots & \frac{u_M}{t - z_M} \end{pmatrix} \geq 0,$$

$$S_2 = \int_0^\infty \begin{pmatrix} \frac{u_1^*}{t - \bar{z}_1} \\ \vdots \\ \frac{u_M^*}{t - \bar{z}_M} \end{pmatrix} t d\mu(t) \begin{pmatrix} \frac{u_1}{t - z_1} & \cdots & \frac{u_M}{t - z_M} \end{pmatrix} \geq 0.$$

Conversely, suppose $S_1 > 0$ and $S_2 \geq 0$. Notice that

$$\begin{cases} A^* S_1 - S_1 A = C_+^* C_- - C_-^* C_+, \\ A^* S_2 - S_2 A = A^* C_+^* C_- - C_-^* C_+ A. \end{cases} \quad (32)$$

$$(33)$$

These equations uniquely determine S_1 and S_2 as the spectra of A and A^* do not overlap. Observe that if S_1 satisfies (32), then $S_2 := S_1 A + C_+^* C_-$ is the solution of (33). Therefore, we have

$$S_2 = S_1 A + C_+^* C_- \quad (34)$$

Note that $S_2 - zS_1 = S_1^{\frac{1}{2}} (S_1^{-\frac{1}{2}} S_2 S_1^{-\frac{1}{2}} - z) S_1^{\frac{1}{2}}$. Since $S_1^{-\frac{1}{2}} S_2 S_1^{-\frac{1}{2}}$ has eigen values in $[0, \infty)$, $(S_1^{-\frac{1}{2}} S_2 S_1^{-\frac{1}{2}} - z)$ is invertible for $z \notin [0, \infty)$. Let (X, D) be the eigen decomposition such that

$$S_1^{-\frac{1}{2}} S_2 S_1^{-\frac{1}{2}} = X D X^* \text{ with } X = (\mathbf{x}_1 \ \cdots \ \mathbf{x}_{qM}), \quad D = \text{diag}(d_j)_{j=1}^{qM}.$$

Then we have for $z \notin [0, \infty)$

$$F(z) = \sum_{j=1}^{qM} \left(\frac{1}{d_j - z} \right) C_+ S_1^{-\frac{1}{2}} \mathbf{x}_j \mathbf{x}_j^* S_1^{-\frac{1}{2}} C_+^*,$$

and thus $F(z)$ has the required form with $d\mu$ being a atomic measure supported on d_1, \dots, d_{qM} .

Furthermore, letting $\mathbf{e}_1, \dots, \mathbf{e}_M$ be the standard basis vectors of \mathbb{R}^M , we have for $i = 1, \dots, M$,

$$(z_i S_1 - S_1 A - C_+^* C_-)(\mathbf{e}_i \otimes I_q) = S_1(z_i - I - A)(\mathbf{e}_i \otimes I_q) - C_+^* C_-(\mathbf{e}_i \otimes I_q) = 0 - C_+^* u_i = -C_+^* u_i.$$

Thus

$$F(z_i) u_i = -C_+(z_i S_1 - S_1 A - C_+^* C_-)^{-1} C_+^* u_i = -C_+(-\mathbf{e}_i \otimes I_q) = v_i. \quad \square$$

To apply this theorem to our problem, we first note that if we identify z in Theorem 2.1 with $-\frac{1}{s}$, then the IRF for $D_j^J(s)$ in (9), denoted by D^J for simplicity, can be written as

$$D^J(s) = (-z) \int_0^{\Theta_1} \frac{d\sigma^J}{t-z},$$

and

$$D^J(s) - \alpha_\infty = (-z) \left(\int_0^{\Theta_1} \frac{d\sigma^J(t)}{t-z} - \frac{\alpha_\infty}{-z} \right) = (-z) \left(\int_0^{\Theta_1} \frac{d\sigma^J(t)}{t-z} - \int_0^{\Theta_1} \frac{\alpha_\infty \sigma(t)}{t-z} \right), \quad (35)$$

where $\sigma(t)$ is a Dirac measure at $t = 0$. Since σ^J has a Dirac measure of strength α_∞ , the function inside the parentheses in (35) is a Stieltjes function, which we denote by $F_{new}(z)$, i.e.

$$D^J(s) - \alpha_\infty = (-z)F_{new}(z)$$

What we would like to harvest is the pole-residue approximation of $D(s) - \alpha_\infty$. To avoid truncation error, we rewrite all the formulas in Theorem 2.1 in terms of variable $s = -\frac{1}{z}$ as follows.

$$s_i = -\frac{1}{z_i}, u_i = \frac{1}{s_i}, \quad (36)$$

$$v_i = D(s_i) - \alpha_\infty, i = 1 \dots M, \quad (37)$$

$$(S_1)_{ij} = \frac{-s_j D(s_j) + s_i^* D^*(s_i)}{s_i^* - s_j}, \quad (38)$$

$$(S_2)_{ij} = \frac{-D(s_j) + D^*(s_i)}{s_j - s_i^*}. \quad (39)$$

Consequently, we have the following representation for $D(s)$

$$D^J(s) \equiv \alpha_\infty + \left(-\frac{1}{s}\right)F_{new}\left(-\frac{1}{s}\right) = \alpha_\infty + \sum_{j=1}^{qM} \left(\frac{-1}{sd_j + 1}\right) C_+ S_1^{-\frac{1}{2}} \mathbf{x}_j \mathbf{x}_j^* S_1^{-\frac{1}{2}} C_+^*. \quad (40)$$

With the generalized eigenvalues $[\mathbf{V}, \mathbf{L}] := eig(S_2, S_1)$, where \mathbf{V} is the matrix of generalized vectors and \mathbf{L} the diagonal matrix of generalized eigenvalues such that

$$S_2 \mathbf{V} = S_1 \mathbf{V} \mathbf{L}, \quad (41)$$

we have

$$D^J(s) = \alpha_\infty + \sum_{k=1}^{qM} \frac{C_+ \mathbf{V}(:, k) \mathbf{V}(:, k)^* C_+^*}{1 + s \mathbf{L}(k, k)}. \quad (42)$$

3 Numerical Examples

In this section, we apply both algorithms in Section 2 to the examples of cancellous bone (S1) studied in [11], [8] and the epoxy-glass mixture (S2 and S3) and the sandstone (S4 and S5) examples studied in [5]. From prior results, it is known that wider range the frequency is, the more ill-conditioned the corresponding matrices will be. We focus on the test case in [5], which apply the fractional derivate approach to deal with the memory term. In this case, time profile of the source term, denoted by $g(t)$ is a Ricker signal of central frequency $f_0 = 10^5 \text{ s}^{-1}$ and time-shift $t_0 = 1/f_0$, i.e.

$$g(t) = \begin{cases} (2\pi^2 f_0^2 (t - t_0)^2 - 1) \exp(-\pi^2 f_0^2 (t - t_0)^2), & \text{if } 0 \leq t \leq 2t_0, \\ 0, & \text{otherwise.} \end{cases}$$

The spectrum content of $g(t)$ is visualized by its Fourier transform $\mathcal{F}\{g\}(\omega)$. Since the real part and the imaginary part is symmetric and anti-symmetric with respect to $\omega = 0$, respectively, we only plot the $\omega \geq 0$ part of the graphs. Based on Figure 2a and Figure 2b, we choose the frequency range in our numerical simulation to be from 10^{-3} Hz to $2 \times 10^6 \text{ Hz}$.

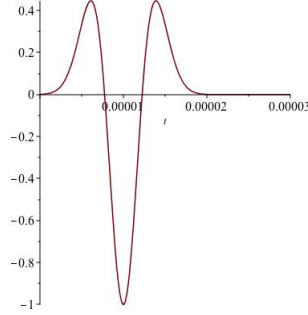


Figure 1: Ricker wavelet $g(t)$

Table 1: Biot-JKD parameters

		S1	S2	S3	S4	S5
$\rho_f(Kg \cdot m^{-3})$	pore fluid density	1000	1040	1040	1040	1040
$\phi(\text{dimensionless})$	porosity	0.8	0.2	0.2	0.2	0.2
$\alpha_\infty(\text{dimensionless})$	infinite-frequency tortuosity	1.1	3.6	2.0	2.0	3.6
$K_0(m^2)$	static permeability	3e-8	1e-13	6e-13	6e-13	1e-13
$\nu(m^2 \cdot s^{-1})$	kinematic viscosity of pore fluid	$1e-3/\rho_f$	$1e-3/\rho_f$	$1e-3/\rho_f$	$1e-3/\rho_f$	$1e-3/\rho_f$
$\Lambda(m)$	structure constant	2.454e-5	3.790e-6	6.930e-6	2.190e-7	1.20e-7

We consider first the equal spaced sample points. Similar to what was reported in [14], the relative error peaked near low frequency. This is due to fact that in general, the function $D(s = -i\omega)$ varies the most near the lower end of ω . This observation leads to the log-distributed grid points, which in general performs better in terms of maximum relative errors but with more ill-conditioned matrices. For both the equally spaced and the log-spaced grids point, ill-conditioned matrices are involved. The ill-conditioning nature of the matrices A in Algorithm 1 and S_1, S_2 in Algorithm 2, together with the fact there is no obvious preconditioner available for these matrices, we resort to the multiprecision package *Advantix* [9] for directly solving (26) and the subsequent partial fraction decomposition involved in Algorithm 1 and for solving the generalized eigenvalue problem (41). These real-valued poles and residues are then converted to double precision before we evaluate the relative errors

$$rel_err(s) := \frac{|D^J(s) - D_{est}^J(s)|}{|D^J(s)|},$$

where the pole-residue approximation function D_{est}^J is defined in (23).

The relative error rel_err with $M = 10$ for all the 5 media listed in Table 1 is plotted in Figure 3a to Figure 3e. The results by using equally space grids are in color blue while those by using log-distributed ones are in color red.

Among all the 5 media listed in Table 1, the sandstones S4 and S5 are the most difficult one to approximate in the sense that it requires the largest M for achieving the same level of accuracy as for other media. Hence we will use S4 to demonstrate the worst case scenario of the performance of our numerical algorithms.

In Table 2, we list the condition numbers for both of the equally-spaced grid points and the log-distributed one. As can be seen, the condition numbers for matrices involved in Algorithm 1 with log-distributed grid points worsen very rapidly with the increase of M and the rescaling of volumes of A is not effective when compared with the equally spaced case. In Figure 4, where the poles and residues for $M = 8$ computed with different combinations of methods are plotted in log-log scale, we see that Algorithm 1 and 2 indeed give numerically identical results. The calculation is carried out by using 90 significant digits and it takes about 5 seconds with a single processor MacBook Pro.

Table 2: Condition numbers of the matrices for material S5

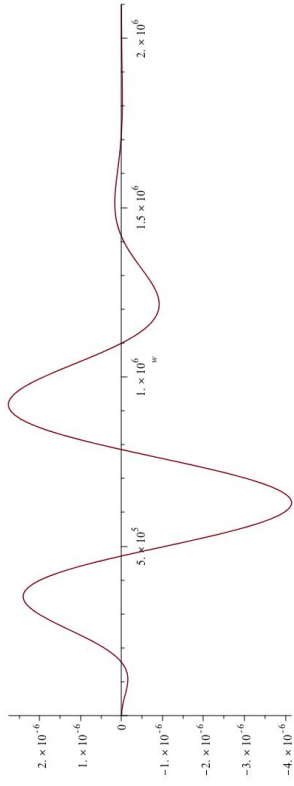
	M=8	M=8	M=14	M=14
	Equally spaced	log-spaced	Equally spaced	log-spaced
A	1.216442e+51	6.712975e+51	7.860543e+88	9.601685e+89
B	1.690184e+12	6.553785e+43	1.441229e+17	8.193134e+80
S_1	2.192279e+11	1.183083e+23	7.157170e+21	1.059471e+47
S_2	7.299177e+13	1.116016e+23	2.143866e+24	9.934587e+46

In Figure 5, the relative error rel_err for approximations by using equally spaced grid and by log-distributed grids are presented. As can be seen from Figure 6a, the peak of error near the lower end of the frequency range is due to the fact that the function being approximated needs more grid points there to resolve the variation. This is achieved by using the log-distributed grids. In Figure 6a and Figure 6b, we plot D^J and its pole-residue approximation D_{est}^J to visualize the performance. Figure 6a corresponds to the equally spaced grids while Figure 6b to the log-distributed one. In both figures, these two functions are almost indiscernible except the imaginary parts in Figure 6a near the lower end of frequency where rel_err peaks; both the colors black (imaginary part of D^J) and green (imaginary part of D_{est}^J) can be seen there.

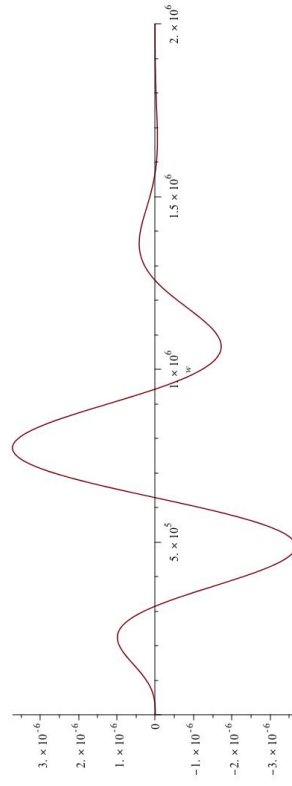
4 Conclusions

In this paper, we utilize the Stieltjes function structure of the JKD dynamic tortuosity to derive an augmented system of Biot-JKD equations (20)-(22) that approximates the solution of the original Biot-JKD equations (2)-(3). Asymptotic behavior of the tortuosity function as $\omega \rightarrow \infty$ is enforced analytically before the numerical interpolation carried out by Algorithm 1 and Algorithm 2. Due to the nature of the tortuosity functions, log-distributed interpolation points generally perform better than the equally distributed ones. We tested our algorithms on 5 sets of poroelastic parameters obtaining from the existing literature and interpolated the JKD dynamic tortuosity equation to high accuracy through a frequency range that spans 9 orders of magnitude from 10^{-3} to 2×10^6 . The extremely ill-conditioned matrices are dealt with by using a multiprecision package *Advansix* in which we set the significant digits of floating numbers to be 90. It turns out Algorithms 1 and 2 are numerically equivalent. We think the exact link between these two algorithms can be derived through the Barycentric forms for rational approximations [3], which in turn provides an algorithm that can adapt the choice of grid points based on the data points so the Lebesgue constant is minimized [13]. This will be explored in a later work.

Acknowledgments. We wish to thank Joe Ball, Daniel Alpay, Marc van Barel, Thanos Antoulas, Sanda Lefteriu, and Cosmin Ionita for their helpful suggestions.

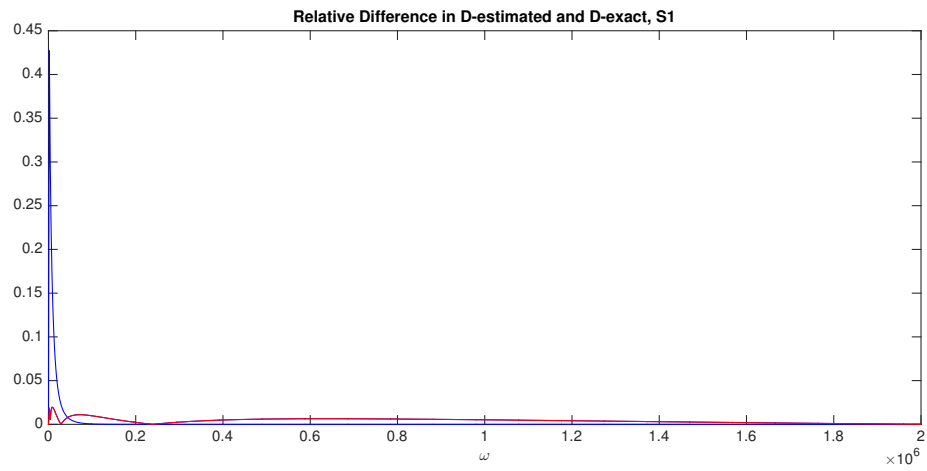


(a) Real part of $\mathcal{F}\{g\}(\omega)$

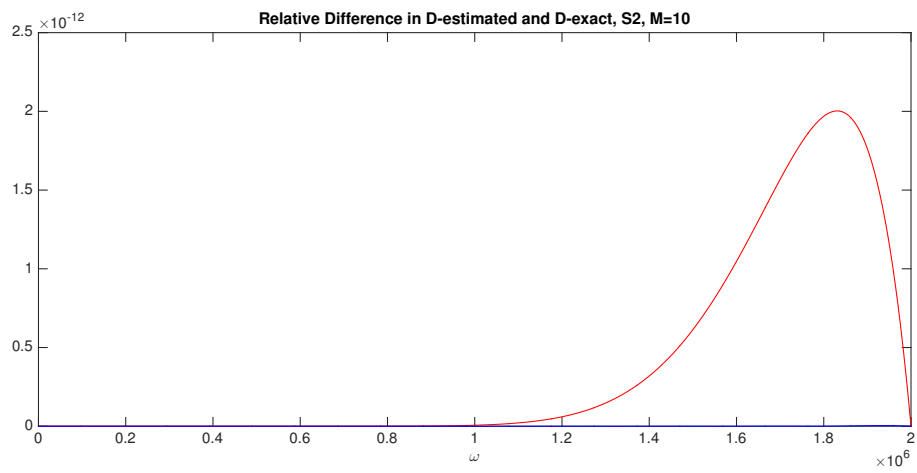


(b) Imag. part of $\mathcal{F}\{g\}(\omega)$

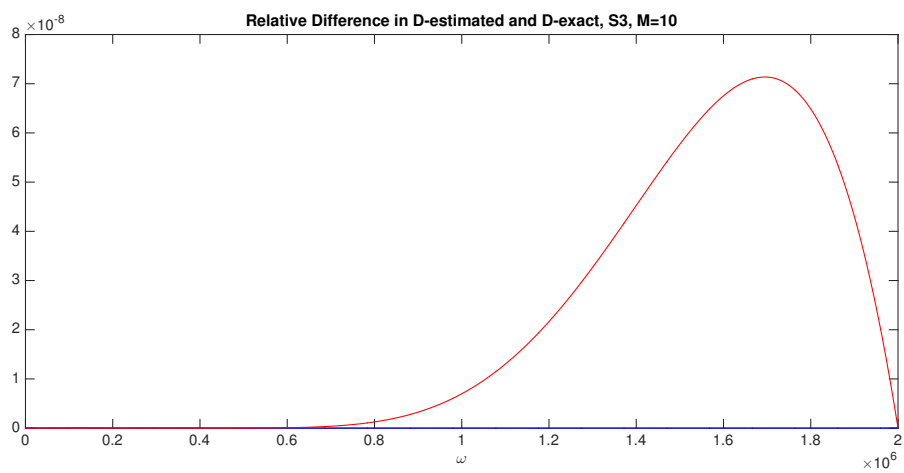
Figure 2: Spectral content of $g(t)$



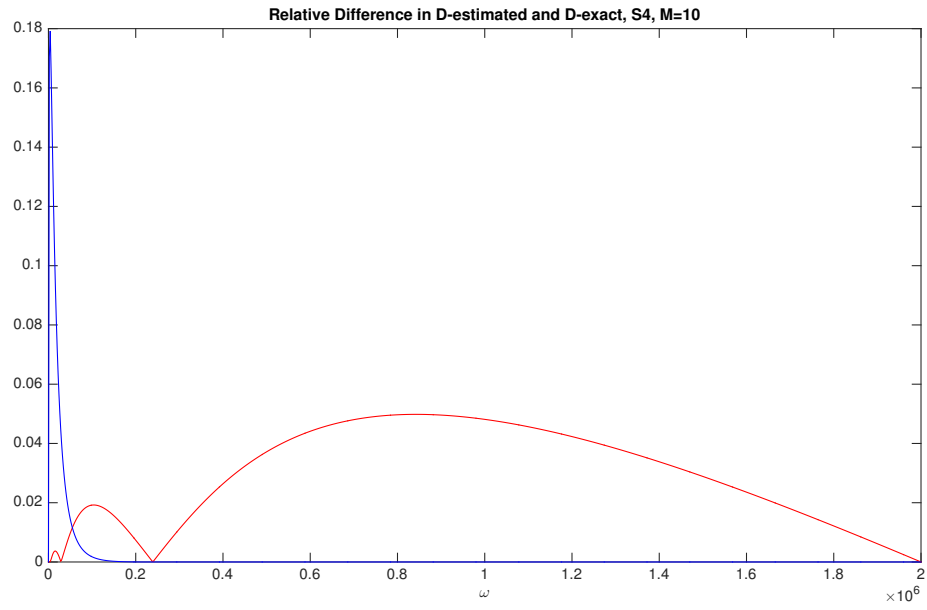
(a) S1



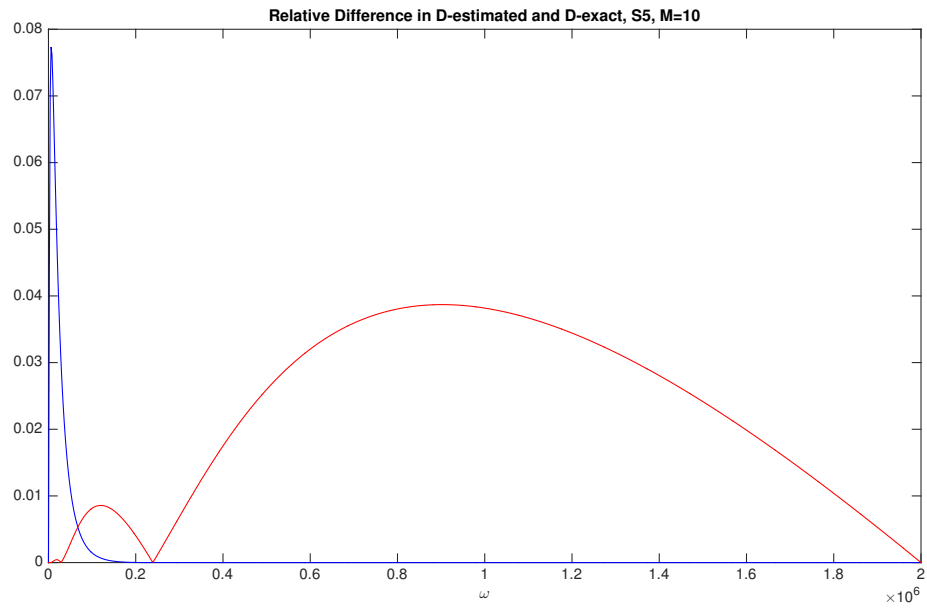
(b) S2



(c) S3



(d) S4



(e) S5

Figure 3: Comparison of relative errors with $M = 10$ for S1 to S5. Blue: Equally spaced grids, Red: log-distributed grids

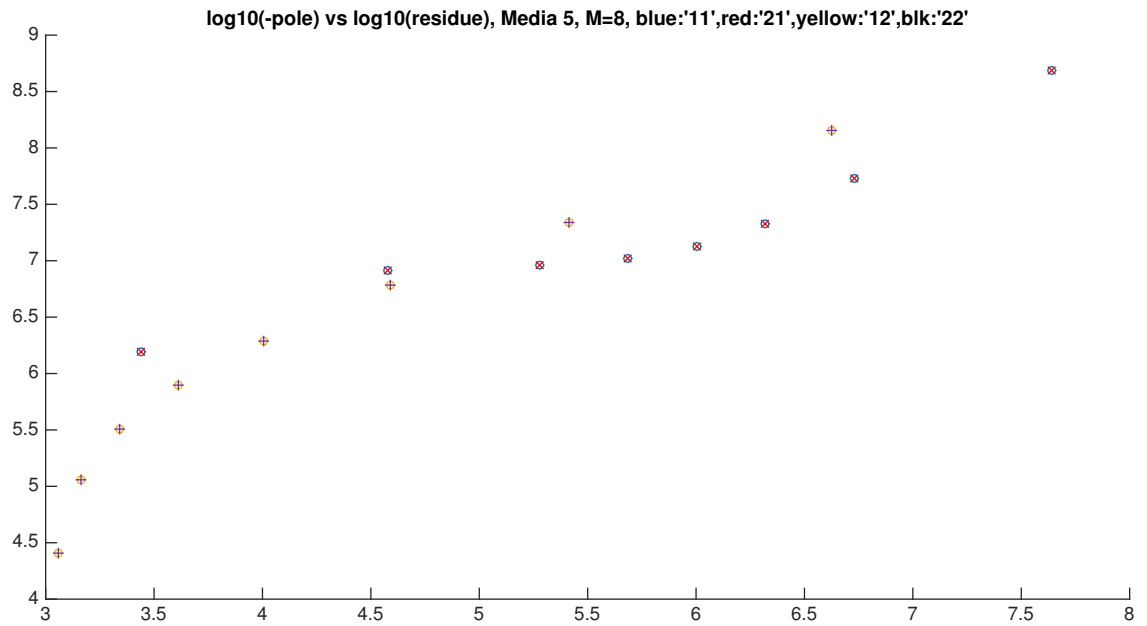


Figure 4: $(\log(-p_k), \log(r_k))$, $k = 1, \dots, 8$. Blue circle: Algo. 1 & equal-space, red cross: Algo. 2 & equal-space, yellow circle: Algo. 1 & log-spaced, green plus: Algo. 2 & log-spaced

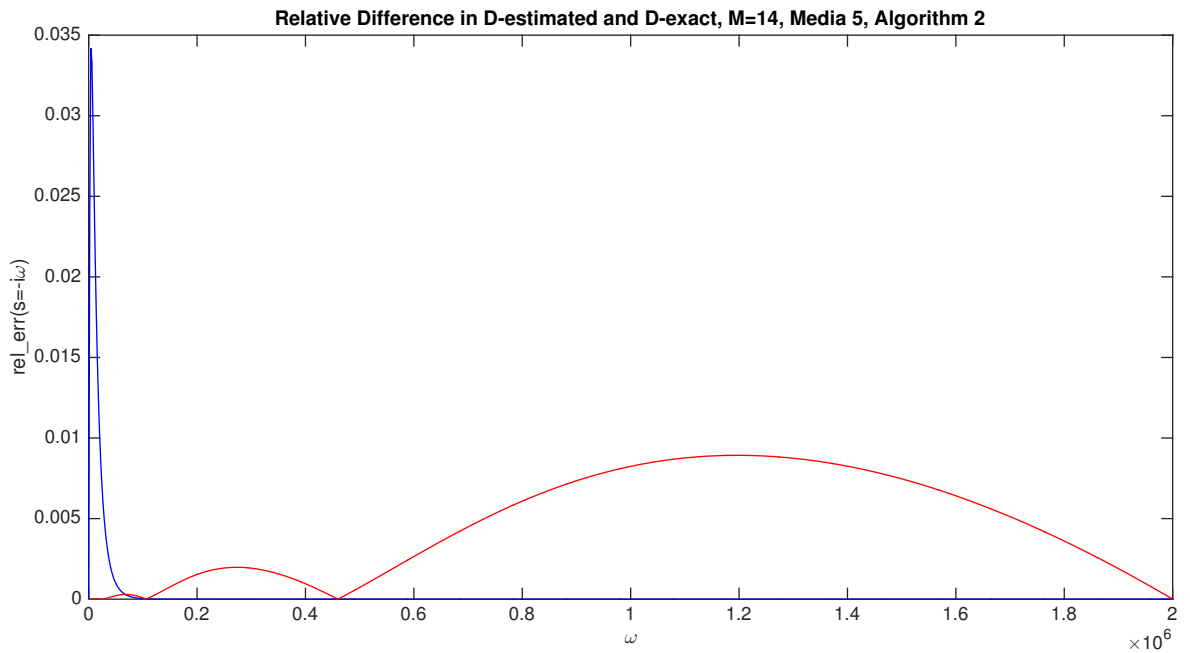
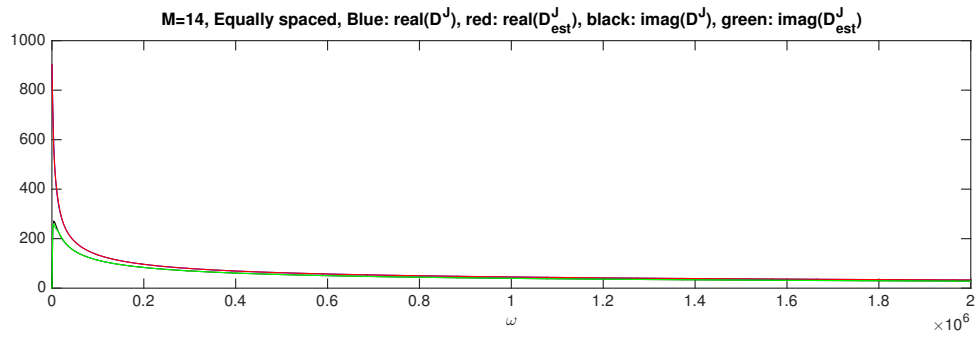
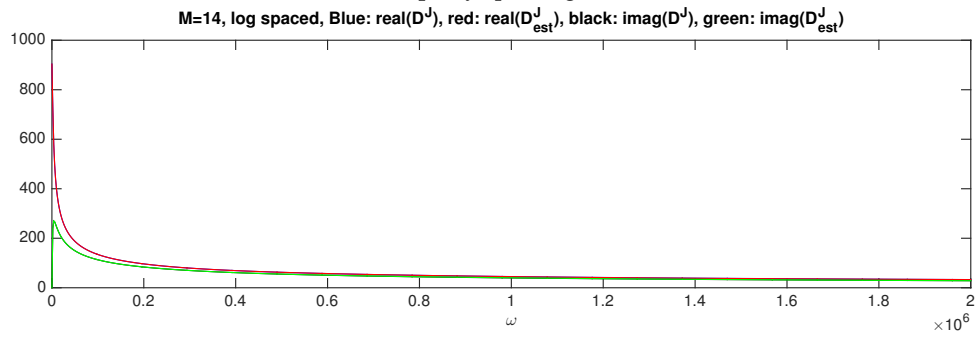


Figure 5: $rel_err(s = -i\omega)$, Blue: equally spaced grids, Red: log-distributed grids



(a) Equally spaced grids



(b) log-distributed grids

Figure 6: Comparison of $D^J(s = -i\omega)$ and $D_{est}^J(s = -i\omega)$. Blue: $\text{real}(D^J)$, Red: $\text{real}(D_{est}^J)$, Black: $\text{imag}(D^J)$, Green: $\text{imag}(D_{est}^J)$

References

- [1] Daniel Alpay, Joseph A Ball, Israel Gohberg, and Leiba Rodman. The two-sided residue interpolation in the Stieltjes class for matrix functions. *Linear algebra and its applications*, 208:485–521, 1994.
- [2] Athanasios C. Antoulas, Sanda Lefteriu, and A. Cosmin Ionita. A tutorial introduction to the Loewner framework for model reduction. In *Model reduction and approximation*, volume 15 of *Comput. Sci. Eng.*, pages 335–376. SIAM, Philadelphia, PA, 2017.
- [3] J-P Berrut and Hans D Mittelmann. Lebesgue constant minimizing linear rational interpolation of continuous functions over the interval. *Computers & Mathematics with Applications*, 33(6):77–86, 1997.
- [4] M.A. Biot. Mechanics of deformation and acoustic propagation in porous media. *Journal of applied physics*, 33(4):1482–1498, 1962.
- [5] Emilie Blanc, Guillaume Chiavassa, and Bruno Lombard. Wave simulation in 2d heterogeneous transversely isotropic porous media with fractional attenuation: A cartesian grid approach. *Journal of Computational Physics*, 275:118–142, 2014.
- [6] J.M. Carcione. *Wave Fields in Real Media: Wave Propagation in Anisotropic, Anelastic and Porous Media*. Pergamon-Elsevier, Oxford, 2001.
- [7] John W. Dettman. *Applied Complex Variables*. Dover publications, 1965.
- [8] Mohamed Fellah, Zine El Abiddine Fellah, Farid G Mitri, Erick Ogam, and C Depollier. Transient ultrasound propagation in porous media using biot theory and fractional calculus: Application to human cancellous bone. *The Journal of the Acoustical Society of America*, 133(4):1867–1881, 2013.
- [9] Multiprecision Computing Toolbox for MATLAB 4.4.7.12736. Advanpix LLC., Yokohama, Japan, 2018.
- [10] JK Gelfgren. Multipoint padé approximants converging to functions of stieltjes’ type. In *Padé Approximation and its Applications Amsterdam*, pages 197–207. Springer, 1981.
- [11] A Hosokawa. Ultrasonic pulse waves in cancellous bone analyzed by finite-difference time-domain methods. *Ultrasonics*, 44:e227–e231, 2006.
- [12] D.L. Johnson, J. Koplik, and R. Dashen. Theory of dynamic permeability and tortuosity in fluid-saturated porous media. *Journal of fluid mechanics*, 176(1):379–402, 1987.
- [13] Yuji Nakatsukasa, Olivier Sète, and Lloyd N Trefethen. The AAA algorithm for rational approximation. *arXiv preprint arXiv:1612.00337*, 2016.
- [14] Miao-Jung Yvonne Ou. On reconstruction of dynamic permeability and tortuosity from data at distinct frequencies. *Inverse Problems*, 30(9):095002, 2014.